Check for updates

Development of a dry powder formulation for pulmonary delivery of azithromycin-loaded nanoparticles

Alison Tatiana Madrid Sani[1,2],
Khellida Loiane V. Ramos-Rocha[1,2], Michelle Alvares Sarcinelli[3],
Marcelo Henrique da Cunha Chaves[3],
Helvécio Vinícius Antunes Rocha[3], Patrícia Léo[1],
Natália Neto Pereira Cerize[1], Maria Helena Ambrosio Zanin[1],
Valker Araujo Feitosa[2]* and Carlota de Oliveira Rangel-Yagui[2]*

[1]Bionanomanufacturing Center, Technological Research Institute, São Paulo, Brazil, [2]Department of
Biochemical and Pharmaceutical Technology, University of São Paulo, São Paulo, Brazil, [3]Laboratory of
Micro and Nanotechnology, Fundação Oswaldo Cruz, Rio de Janeiro, Brazil

The COVID-19 pandemic has raised concern regarding respiratory system diseases and oral inhalation stands out as an attractive non-invasive route of administration for pulmonary diseases such as chronic bronchitis, cystic fibrosis, COVID-19 and community-acquired pneumonia. In this context, we encapsulated azithromycin in polycaprolactone nanoparticles functionalized with phospholipids rich in dipalmitoylphosphatidylcholine and further produced a fine powder formulation by spray drying with monohydrated lactose. Nanoparticles obtained by the emulsion/solvent diffusion-evaporation technique exhibited a mean hydrodynamic diameter around 195−228 nm with a narrow monomodal size distribution (PdI < 0.2). Nanoparticle dispersions were spray-dried at different inlet temperatures, atomizing air-flow, aspirator air flow, and feed rate, using lactose as a drying aid, resulting in a maximal process yield of 63% and an encapsulation efficiency of 83%. Excipients and the dry powder formulations were characterized in terms of morphology, chemical structure, thermal analyses and particle size by SEM, FTIR, DSC/TGA and laser light diffraction. The results indicated spherical particles with 90% at 4.06 μm or below, an adequate size for pulmonary delivery. Aerosolization performance in a NGI confirmed good aerodynamic properties. Microbiological assays showed that the formulation preserves AZM antimicrobial effect against *Staphylococcus aureus* and *Streptococcus* pneumoniae strains, with halos above 18 mm. In addition, no formulation-related cytotoxicity was observed against the human cell lines BEAS-2B (lung epithelial), HUVEC (endothelial) and HFF1 (fibroblasts). Overall, the approach described here allows the production of AZM-PCL nanoparticles incorporated into inhalable microparticles, enabling more efficient pulmonary therapy of lung infections.

KEYWORDS

spray-drying, polycaprolactone, azithromycin, dry powder inhaler, pulmonary diseases

Introduction

Respiratory diseases, such as chronic bronchitis, tuberculosis, cystic fibrosis, obstructive pulmonary disease (COPD), COVID-19 and community-acquired pneumonia (CAP) mainly involve the lungs and represent the second cause of death in the world [1]. In particular, CAP refers to pneumonia occurring outside of a hospital and may result from serious respiratory tract infections caused by bacteria, fungus or viruses in children and older adult [2, 3]. The most common treatment for bacterial respiratory infections is the oral administration of high doses of antibiotics, in particular azithromycin (AZM) [4], a macrolide with a broad antibacterial spectrum and high activity against gram-negative and gram-positive organisms [5]. It also presents anti-inflammatory and immunomodulatory properties. Nonetheless, oral administration of AZM can cause nausea, vomiting, diarrhea, and abdominal pain, especially in children [6]. The most common adverse effects associated with AZM involve the gastrointestinal tract and the central and peripheral nervous system [7]. In addition, we can mention severe dizziness, headache, fatigue, and cutaneous manifestations. Less common but serious side effects such as liver damage occur because AZM has become commonly used [8]. Abnormal heart rhythm changes including ventricular arrhythmias may also occur owing to the potential to prolong the QT interval [9]. In some rare cases AZM is associated with an increased risk of cardiovascular death [10]. Therefore, alternative routes of administration such as the pulmonary could benefit patients treated with AZM.

The inhalation route has several advantages when compared to the oral and parenteral routes such as avoiding first-pass hepatic metabolism, rapid diffusion in the lower airways, faster local therapeutic action and higher efficacy, lower doses, and therefore, less direct exposure of other organs to the drug and reduction of side effects [11]. Dry powder inhalers (DPIs) represent the most promising devices for pulmonary administration of drugs. They are safer to the environment since propellant gases are not used and are relatively easy to use by the population [12]. The success of this type of formulation, i.e., maximal deposition in the lower airways, depends on the dry powder properties such as composition, size (below 5 μm), surface morphology and aggregation [13]. A rapid, economic and scalable technique to produce adequate dry powders refers to spray drying, a process in which a dispersion is converted into small droplets to be dried in a hot air chamber [14, 15]. With the proper selection of process conditions, a homogenous powder with optimal particle characteristics can be obtained.

In this work, AZM-loaded nanoparticles of polycaprolactone (AZM-PCL-NPs) functionalized with phospholipids rich in dipalmitoylphosphatidylcholine were prepared by emulsion/solvent diffusion-evaporation technique and the colloidal dispersion was further used to produce AZM-loaded microparticles of polycaprolactone (AZM-PCL-MPs), with lactose as a drying aid, using spray-drying process, resulting in a final dry powder formulation of nano-in-microparticles with adequate size for pulmonary delivery.

Materials and methods

Preparation of AZM-PCL nanoparticles (NPs)

AZM-PCL-NP were produced by emulsion/solvent diffusion-evaporation technique. This method involves three main steps, emulsification 1): both the drug and the encapsulating polymer are dissolved in an organic solvent followed by homogenization in an aqueous solution with a dispersing agent forming nanometric droplets. The next step involves diffusion 2): solvent diffuses from the organic phase of the emulsion by the addition of water in excessive quantities resulting in the precipitation of the polymer in the droplets thus producing a dispersion of NPs. Further, the dispersion is subjected to evaporation 3): the solvent is removed under reduced pressure resulting in an aqueous dispersion of NPs.

In detail, the organic phase containing AZM dihydrate (Pliva, Croatia), PCL (10 kDa, Sigma Aldrich, United States) and soybean lecithin S75® (phospholipids rich in dipalmitoylphosphatidylcholine-DPPC, Lipoid, Germany), from now referred as DPPC, were dissolved in 25 mL of ethyl acetate in an ultrasound bath (P30 kHz, Elma, Germany) at 50°C during 25 min in the molar ratio of AZM:PCL:DPPC (0.06, 0.19, 0.75). This phase was added slowly to 100 mL aqueous solution of Pluronic® F127 (10 mg/mL) (EO/PO/EO triblock copolymer, 80% EO, 8400 MW, Sigma Aldrich, United States) and emulsified by 5 min at 14,000 rpm in an Ultra-turrax® (IKA, Germany). Then, 150 mL deionized water was added as a dilution phase, allowing the diffusion of ethyl acetate from the organic phase to the aqueous phase. The resulting dispersion was evaporated at 50°C, 100 rpm, under reduced pressure (45 mbar) in a rotary evaporator R-215 (Büchi, Switzerland) to remove the organic solvent, resulting in AZM-PCL-NP formulations. Furthermore, placebo nanoparticles (PCL-NP) were prepared for comparison purposes.

Characterization and stability of the nanoparticles

The PCL-NP and AZM-PCL-NP dispersions were stored in a refrigerator (4°C) and analyzed periodically (at least once a week) for size and polydispersity. Particle size and polydispersity index (PdI) were determined by dynamic light scattering (DLS) measurements on a NanoPlus Zeta/nano analyzer (Micrometrics, Georgia, United States). Samples (20 μL) were diluted in 1 mL of purified water. Results are presented as the mean and standard deviation of three independent measurements (n = 3).

TABLE 1 AZM-PCL-MP formulation yield (%) during the spray-drying process.

Run	Inlet temperature (°C)	Outlet temperature (°C)	Atomizing air flow (LN/h)	Aspirator air flow (%)	Feed rate (mL/min)	Process yield (%)
1	80	57	600	80	5.81	41*
2	80	55	600	70	5.95	38*
3	100	64	600	80	4.72	51
4	100	64	600	70	4.55	63
5	110	54	800	80	7.35	57
6	110	49	800	70	7.27	55
7	120	61	800	80	4.63	58
8	120	59	800	70	4.60	58

*The obtained powder melted inside the spray-drying chamber.

Preparation of the dry powder inhalable microparticles (MPs)

In order to get dry powder MPs by spray-drying method, micronized lactose monohydrate (Lactohale® LH206, DFE Pharma, Germany) was used as a thermic protector for PCL-NP and AZM-PCL-NP dispersions. During NPs preparation (*vide* 2.1.), lactose was solubilized in dilution phase at 0.25, 0.5, 0.75 or 1 wt%. Immediately before evaporation step, the PCL-NP and AZM-PCL-NP dispersions were pumped into a spray-dryer (mini B190, Büchi, Cleveland, United States) filled with a stainless steel standard fluid nozzle tip of 0.5 mm internal diameter. Conditions such as inlet temperature, outlet temperature, atomizing air flow, aspirator air flow and feed rate were investigated (Table 1) to generate the PCL microparticulate powder (PCL-MP) and the AZM loaded powder (AZM-PCL-MP). After spray drying, powder formulations were kept in a desiccator at room temperature. Process yield (%) was calculated with Equation 1, which refers to the weight percentage of the powder collected in relation to the initial weight of the solids dissolved in the feed solution.

$$\text{Process yield (\%)} = \frac{Amount\ of\ total\ solids\ after\ spray-drying}{Amount\ of\ total\ solids\ before\ spray-drying} \times 100$$

(1)

Physicochemical characterization of the dry powder inhalable microparticles

Field emission electron microscopy SEM-FEG

A High-resolution Field Emission Gun Scanning Electron Microscope (FEG-SEM, 3D FEG, Quanta, United States) at 20 kV was used to investigate the microparticle's morphology. Powder samples (PCL-MPs and AZM-PCL-MPs) were loaded by light dusting onto a metal stub with a double-sided adhesive

carbon tape. The samples were coated with palladium (10 nm) with a sputter coater (TN-1100X-SPC-16M, Canada), using an electric potential of 2.0 kV for 2 min. Microscopic images were randomly captured at various magnifications from 500 to 25,000x.

Laser light diffraction

The AZM-PCL-MPs and PCL-MPs formulations were resuspended (ca. 0.4 wt%) in distilled water as a dispersing medium, with a refractive index of 1.33. The analyses were carried out in Mastersizer MicroPlus (Malvern, United Kingdom) using a Hydro 2000 G (A) dispersion cell.

Differential scanning calorimetry (DSC)

DSC analyzes were carried out using a DSC822 (Mettler-Toledo, Switzerland). Approximately 3–5 mg of the powdered sample (AZM-PCL-MP) and pure excipients were sealed into standard aluminum pans using a pin holed standard aluminum lid. All samples were scanned in the range of 25°C–500°C at a scanning speed of 10°C/min under 50 mL/min nitrogen gas purging using an empty aluminum pan as reference. Thermograms data were collected using the STARe SW thermal analysis software (Mettler Toledo, Switzerland).

Thermogravimetric analysis (TGA)

TGA were conducted using a TGA/DSC 1 STARe System (Mettler-Toledo, Switzerland). Samples of approximately 10 mg of AZM-PCL-MPs were loaded into the platinum pan and analyzed in ramp heating mode at 10°C/min from 25°C to 500°C under nitrogen gas purging of 50 mL/min. The percentage of weight variation upon heating was estimated using the Universal Analysis 2000 software (Mettler Toledo, Switzerland).

X-ray powder diffraction (XRPD)

The crystallinity of the microparticles was analyzed using an X-ray diffractometer (Rigaku, United States) equipped with a Cu-Kα radiation source and a fixed monochromator. The powder

samples of AZM-PCL-MPs were placed in glass holders and X-ray diffraction was measured in the range of 5°–40° 2θ at a scan speed of 5°/min and a step of 0.02°. The voltage and current used were 40 kV and 30 mA, respectively.

Attenuated total reflectance and Fourier transform infrared spectroscopy (ATR-FTIR)

ATR-FTIR spectra were acquired using a Nicolet Is10 Spectrometer (ThermoFisher, United States) in the % transmittance mode. The samples (AZM-PCL-MPs and pure excipients) were placed on the ATR diamond crystal with the pressure arm positioned over the sample and spectra were collected at a resolution of 4 cm^{-1} with 64 scans per spectrum over the range 4,000–700 cm^{-1}. An unsampled background spectrum was collected before each test. All spectra data were collected using ResolutionPro (5.2.0, Agilent Technologies software).

Determination of azithromycin loading and encapsulation efficiency

Drug loading and encapsulation efficiency were determined by a modified spectrophotometric method [16, 17]. Briefly, AZM-PCL-MP were dissolved (ca. 0.99 wt%) in 1 mL dimethylsulfoxide (DMSO) and then mixed with 9 mL methanol. After centrifugation at 24,104 × g for 15 min, the supernatant was collected and diluted in PBS (pH 7.2, 50 mM). Then, 5 mL of diluted solution was added to 5 mL of H_2SO_4 (13.5 M) and allowed to react for 30 min to produce a yellow color. The solution was analyzed at 482 nm in a spectrophotometer (UV/Vis, M-51 BEL$^{®}$ Engineering Photonics) to determine the AZM concentration based on a

standard curve (Figure 1). The encapsulation efficiency (EE%) was calculated with the help of Equation 2 [5].

$$EE\,(\%) = \frac{L_a}{L_t} \times 100 \qquad (2)$$

where L_a is the total mass of AZM encapsulated and L_t is the initial AZM mass added to the system.

In vitro aerosolization performance by next-generation impactor (NGI$^{®}$)

The *in vitro* aerosolization profile of the microparticles was evaluated using a Next-Generation Impactor (NGI$^{®}$, Nottingham, United Kingdom). Size 4 hard gelatin capsules (InfinityPharma, Brazil) were filled with 25 mg of the mixture of AZM-PCL-MPs with micronized lactose LH206 in a 50: 50 ratio. Next, the powder capsules were incorporated into the Aerolizer$^{®}$ dry powder inhalation (DPI) device and punctured once. A flow rate of 100L/min was used, which was supplied by two pumps in series (HCP5, UK) and measured using a flow meter (Copley, Nottingham, DFM2000, Copley, United Kingdom). The flow rate generated a pressure drop of 4 KPa across the inhaler device. The execution time for each experiment was set at 2.4 s to simulate *in vivo* inspiration volume (i.e., 4L). The powder collected inside each one of the plates of NGI was dissolved in DMSO and AZM was quantified by UV-Vis. For the NGI flow rate of Q = 100 L/ min, the effective aerodynamic cutoff diameter (D_{a50}) for each impactor stage was calibrated by the manufacturer and stated as: stage 1, 6.12 μm; stage 2, 3.42 μm; stage 3, 2.18 μm; stage 4, 1.31 μm; stage 5, 0.72 μm; stage 6, 0.40 μm; and stage 7,
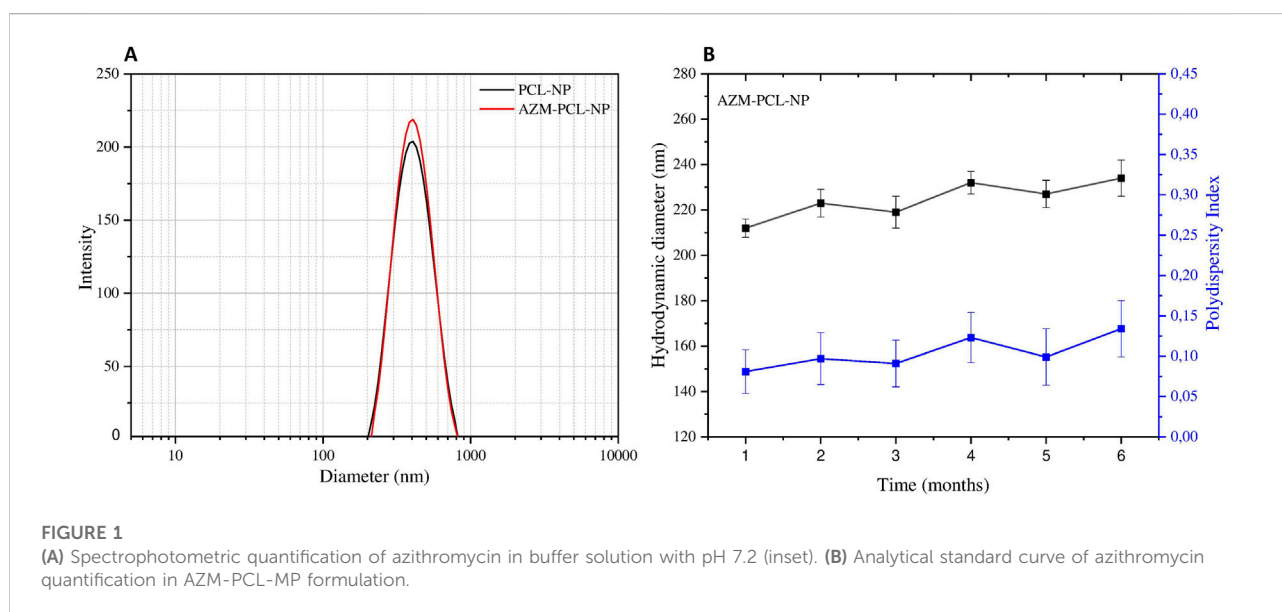

FIGURE 1
(A) Spectrophotometric quantification of azithromycin in buffer solution with pH 7.2 (inset). **(B)** Analytical standard curve of azithromycin quantification in AZM-PCL-MP formulation.

0.24 µm. The emitted dose (ED) was determined as the difference between the initial mass of powder loaded in the capsules and the remaining mass of powder in the capsules following aerosolization. The ED (%) (Equation 3) was used to express the percentage of ED based on the total dose (TD) used [18].

$$Emitted\ Dose\ (ED\%) = \frac{ED}{TD} \times 100\% \qquad (3)$$

The fine particle dose (FPD) was defined as the dose deposited on Stages 2–7 and the fine particle fraction (FPF%) (Equation 4) was expressed as the percentage of FPD to ED.

$$Fine\ Particle\ Fraction\ (FPF\%) = \frac{FPD}{ED} \times 100\% \qquad (4)$$

The respirable fraction (RF%) Equation 5 was used as the percentage of FPD to total deposited dose (DD) on all impactor stages.

$$Respirable\ Fraction\ (RF\%) = \frac{FPD}{DD} \times 100\% \qquad (5)$$

Furthermore, the mass median aerodynamic diameter (MMAD) of aerosol particles was determined based on the cumulative particle size distribution functions obtained from the NGI data. The experiment was carried out, filling 5 capsules one by one, manually and containing 25 mg of powder formulation in each, to guarantee an adequate amount for quantification by UV-Vis.

Cytotoxicity assay

Human bronchial epithelial cell line (BEAS-2B, BCRJ code 0395, Brazil), human fibroblast cell line (HFF-1, ATCC SCRC-1041, United States) and human endothelial cell line (HUVEC, ATCC CRL-1730, United States) were used to investigate the cytotoxicity of AZM, AZM-PCL-NPs and PCL-NPs formulations. The cells were grown in DMEM supplemented with 10% FBS, in an incubator at 37°C, 95% humidity and 5% CO_2 atmosphere. The cell lines were plated at a concentration of 1.5×10^4 cells/well in a 96-well plate. After incubation for 24 h, the cells were exposed to the AZM or AZM-PCL-NP at different concentrations ranging from 25 µg/mL to 1,600 µg/mL to of AZM for EC50 determination. Cell viability was evaluated based on the MTT (3-(4,5-dimethylthiazol-2-yl)-2,5-diphenyltetrazolium bromide) method based on Mosmann [19]. Briefly, 5 mg/mL MTT solution (Invitrogen, United States) and culture medium at 1:10 ratio were added. The cells were then incubated at 37°C for 3 h. After this time, the medium containing the MTT was removed and 200 µL DMSO was added to solubilize the formazan crystals. Cell viability was determined by absorbance spectroscopy at 595 nm. This assay was performed as 3 independent experiments, each in triplicate.

Data analyses were carried out using the Prism 5.0 program and EC50 values were calculated for each cell line studied.

Antimicrobial activity

The antibacterial efficacy of AZM, AZM-PCL-NP and PCL-NP formulations was evaluated *in vitro* against *Streptococcus pneumoniae* (ATCC 6303) and *Staphylococcus aureus* (ATCC 6538). All microbiological tests were performed in triplicate and results are presented as mean and standard deviation. *S. pneumoniae* strain was maintained in trypticase soy broth (TSB) or trypticase soy agar (TSA) [20] and the *S. aureus* strain in nutrient broth or nutrient agar [21] prepared according to the manufacturer's instructions. *S. pneumoniae* was kept in microaerophilic environment generation system anaeropack in all tests.

Antimicrobial activity by disk diffusion assay

Petri dishes containing nutrient agar and potato-sucrose-agar were seeded with 10^6 cells of *Staphylococcus aureus* and *Streptococcus pneumoniae*, respectively. In sequence, 6 mm discs impregnated with 20 µL of the respective serial dilutions from 25 to 1,600 µg/mL of AZM, AZM-PCL-NP, PCL-NP were placed in Petri dishes and kept at 37°C for 18 h to analyze bacterial growth and halo formation. Microbiological tests were performed in triplicate [22].

Resazurin bacterial susceptibility test

Samples of 10^6 bacterial cells were plated in 96-well plates and submitted to AZM, AZM-PCL-NP, PCL-NP. The drug concentration ranged from 25 to 1,600 µg/mL and the strains were kept in an incubator at 37°C for 24 h. Two hundred microliters of sterile water was added to all perimeter wells to avoid evaporation during the incubation. After 24 h, 10 µL of resazurin (1 wt%) was added to each well and after 1 h cell viability was observed through color change. A change in color from blue (oxidized state non-viable cell) to pink (i.e., reduced viable cell) indicated bacterial growth [23, 24].

Determination of the minimum inhibitory concentration (MIC)

To determine the minimum inhibitory concentration (MIC) of AZM and AZM-PCL-NP formulation, microdilution was performed in 96-well plates containing 10^6 cells/well of *S. aureus* [20, 25] and *S. pneumoniae*. The AZM concentration ranged from 25 to 1,600 µg/mL. After microdilution in broth, each well with the respective treatment was seeded in Petri dishes with TSA and nutrient agar, for *S. pneumoniae* and *S. aureus*, respectively. After incubation for 24 h at 37°C, the colony forming unit (CFU) count was performed and the minimum concentration required to inhibit bacterial (i.e., CIM) in both strains was calculated.

Results and discussion

Production and characterization of AZM-PCL-NPs

Dynamic light scattering

The scattering profiles of PCL-NP containing or not AZM are presented in Figure 2A. As can be seen, the placebo PCL-NPs presented mean hydrodynamic diameter of 228 ± 8 nm, while the AZM-loaded formulations (AZM-PCL-NPs) presented mean hydrodynamic diameter around 195 ± 12 nm. The corresponding polydispersity index (PdI) were 0.099 ± 0.047 and 0.137 ± 0.032, respectively, indicating homogenous monodisperse systems. These values are similar to previous ones reported in the literature for PCL nanoparticles prepared by the emulsion/solvent diffusion-evaporation method, corresponding to structures of 180–250 nm [26]. The small size and narrow size distribution can be related to the NP preparation method, such as emulsification-diffusion-evaporation. The ratio between components of the organic phase, high shear speed (i.e., 14,000 rpm) promotes the breakage of droplets into smaller ones, resulting in a narrow size distribution [27]. The use of surfactant copolymer (i.e., Pluronic F-127) stabilizes the interface between the organic and aqueous phase, preventing droplet coalescence during emulsification process. Maintaining the aqueous phase in excess can favor the efficient diffusion of the solvent into the aqueous phase, facilitating the formation of homogenous NPs. Finally,
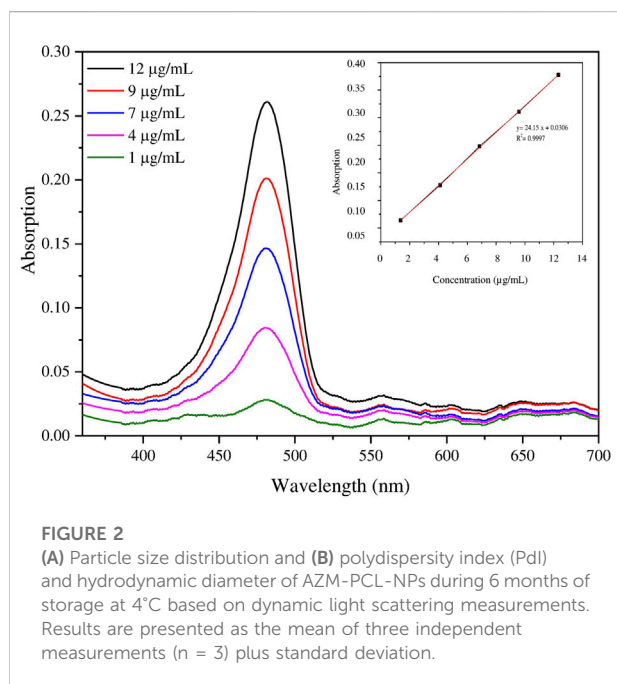
conducting the diffusion and evaporation processes at low temperature (i.e., 50°C) allows the formation of more uniform NPs [28].

This approach also allowed us to achieve a high AZM encapsulation efficiency (%EE) of 83%. The adequate molar proportion of AZM, PCL and DPPC (0.06:0.19:0.75) in the AZM-PCL-NP formulation favored the formation of homogeneous and stable droplets, avoiding particle aggregation and promoting better drug retention inside the NPs, resulting in a high EE%. The adequate ratio of AZM:PCL provided the necessary polymeric matrix to encapsulate AZM, while DPPC stabilized the particle structure without compromising encapsulation. Besides, Pluronic F127 used as a polymeric surfactant also stabilized the emulsification and diffusion process, preventing particle coalescence and resulting in homogeneous particles, favoring high %EE [29, 30]. A high drug encapsulation efficiency of 84% for paclitaxel was also achieved using PLGA-PCL microparticles [31].

Production of PCL-MP and AZM-PCL-MP inhalable powders

Spray-drying is a versatile process to dry polymeric nanostructures and parameters such as inlet temperature, atomizing air flow, aspirator air flow and consequently the feed rate, can be studied [15]. Usually, inlet temperatures from 120°C to 125°C are used [17], nevertheless inlet temperatures from 80–120°C were also previously tested and resulted in compact and homogenous powders [32].

Regarding the use of micronized lactose LH206 as a drying adjuvant, the lactose melted inside the spray-dryer when used at concentrations between 0.25% and 0.75%, probably because the inlet temperatures was too high for this concentration. However, at 1%, lactose contributed to a more stable formulation, producing a homogeneous powder, probably due to the formation of a film around the NPs.

As can be seen in Table 1, run 1 and run 2 resulted in the lowest yields, owing to the higher deposition of the powder on the cyclone walls that was apparent during the production process. The best yield of 63% was obtained for run 4 and corresponded to a higher outlet temperature of 64°C, inlet temperature of 100°C, atomizing air flow in 600 NL/h, aspiration air flow in 70% and feed rate of 4.55 mL/min, which resulted in a homogenous white powder. Inlet temperature at 100°C and the outlet temperature around 64°C, can help prevent AZM degradation while ensuring proper water evaporation. For PCL, these inlet/outlet temperatures allowed it to remain in a solid state, ensuring that the microparticles do not coalesce or lose their structural integrity during drying [33].
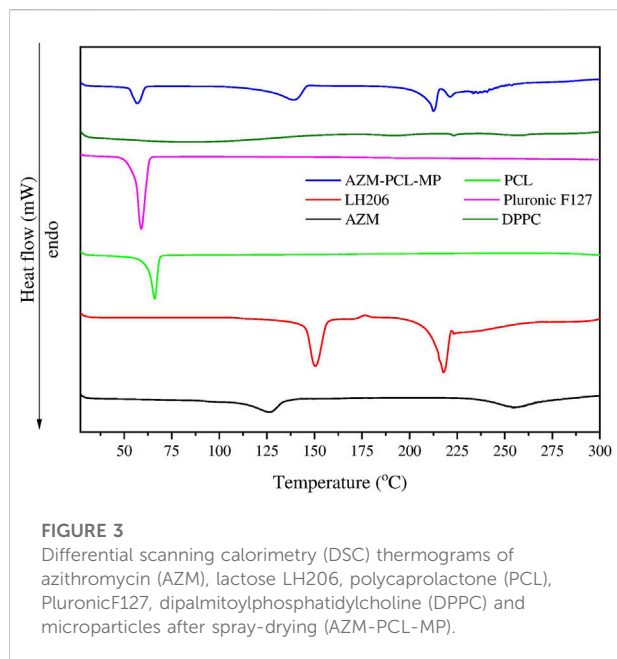

FIGURE 2
(A) Particle size distribution and **(B)** polydispersity index (PdI) and hydrodynamic diameter of AZM-PCL-NPs during 6 months of storage at 4°C based on dynamic light scattering measurements. Results are presented as the mean of three independent measurements (n = 3) plus standard deviation.

FIGURE 3
Differential scanning calorimetry (DSC) thermograms of azithromycin (AZM), lactose LH206, polycaprolactone (PCL), PluronicF127, dipalmitoylphosphatidylcholine (DPPC) and microparticles after spray-drying (AZM-PCL-MP).

Characterization of the AZM-PCL-MP inhalable powder

Thermal analysis (DSC/TGA)

DSC analysis was performed on the raw materials (AZM and excipients) as well the AZM-PCL-MPs to confirm the successful loading of the drug into the formulation (Figure 3). According to previous reports, the melting temperature (T_m) of PCL was demonstrated to be 60°C–71°C [34, 35]. In this study, the endothermic peak of PCL was observed at 66°C. The T_m value of Pluronic F127 obtained in this work, 57°C, is similar to that reported by Karolewicz et al. [36]. For DPPC, no thermal event was observed in the range of 25°C–300°C, which has already been verified by Eedara et al. [37]. On the other hand, the lactose LH206 presented the T_m at 221°C. Listiohadi et al. [38] reported another thermodynamic event of exothermic nature for lactose in the range of 150°C–175°C, which suggests a possible recrystallization of the amorphous phase. We observed this transition around 176°C. AZM presented a T_m value of 126.4°C, which is also closer to the value reported by Maswadeh et al. [39] at 125°C. Furthermore, another thermodynamic event can be observed around 260°C, which can be attributed to the AZM degradation temperature (Td).

For the AZM-PCL-MP (Figure 3), the endothermic peak shifted to a lower temperature of 57°C, corresponding to the T_m of PCL and Pluronic F127 and indicating the miscibility of both polymers in the formulation. Endothermic events at 132°C and 212°C can be attributed to lactose monohydrate, present in higher proportion in the formulation. The endothermic peak corresponding to the Tm of AZM (126°C) was not observed, indicating that the AZM is dispersed in the polymeric nanoparticle matrix [33]. Contribu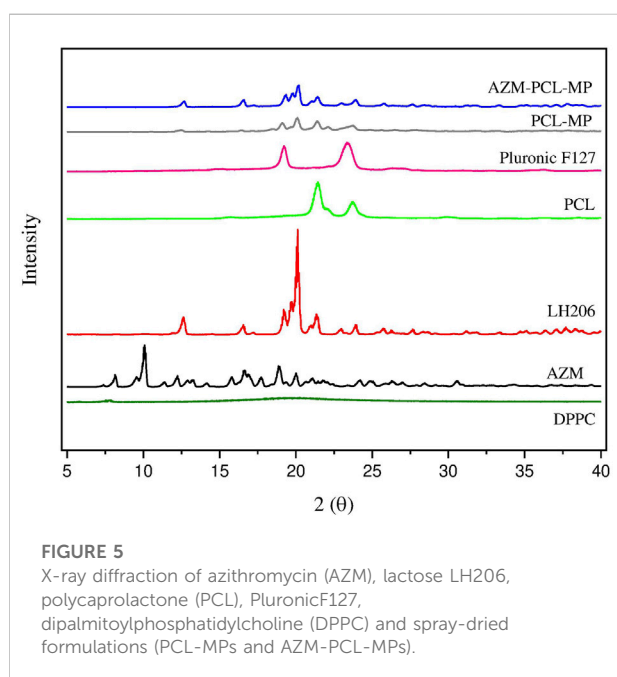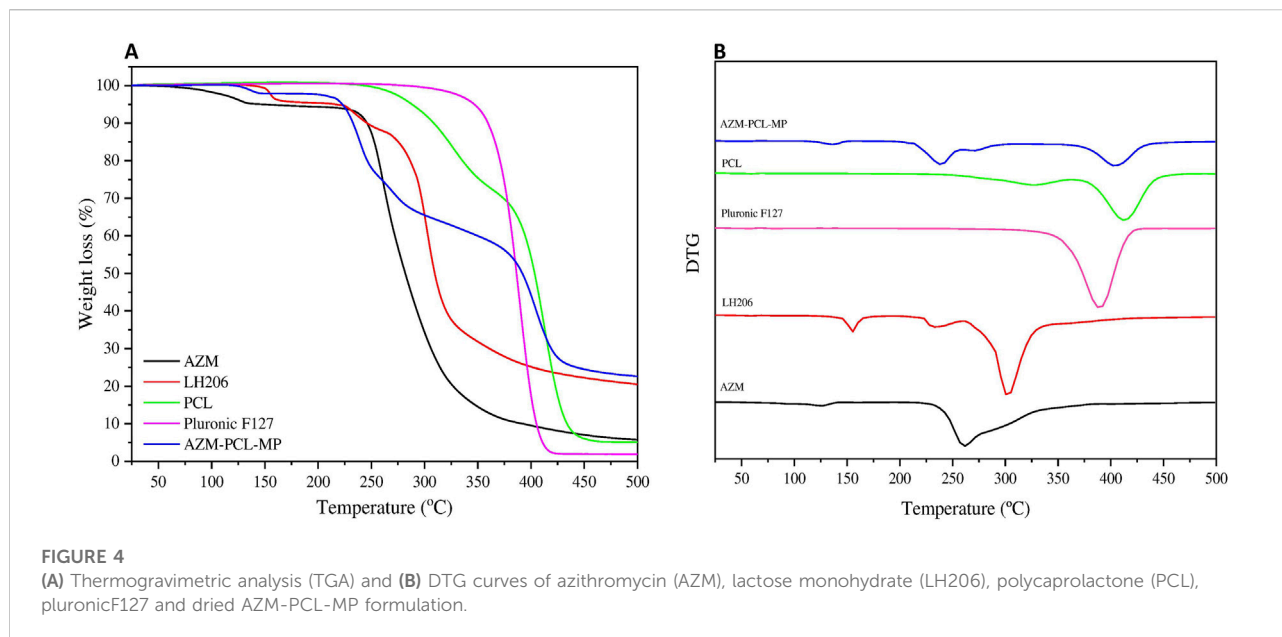tions from the NP formation process may result in the absence of the AZM melting peak, such as the interactions between AZM and the PCL matrix, which stabilize the drug in the amorphous form [40]. The spray-drying process also promotes rapid drying of NPs, preventing recrystallization of AZM. Lactose, which acts as a drying aid and can improve the distribution of AZM in the matrix [41]. Therefore, the resulting formulation presents a molecular or solid dispersion of AZM, which explains the absence of the AZM melting peak in the DSC analysis.

The TGA curves (Figure 4A) represent the thermal degradation of the components (AZM and excipients) and the spray-dried AZM-PCL-MPs. The PCL thermogram showed two events of degradation at 325°C and 410°C. Pluronic F127 thermograms showed one-step process of thermal decomposition at 389°C, corroborating with previous results [33]. AZM presented thermal degradation at 260°C, reaffirming results of DSC analysis [37]. The TGA curve for LH206 showed a minimum loss of mass (ca. 0.4%) between 40°C and 130°C which corresponds to the loss of water at the surface, while a second mass loss (ca. 5.1%) around 153°C, indicating a loss of hydration water [42]. The TGA curve for spray-dried AZM-PCL-MPs remained constant up to 120°C where loss of water was observed. A second event occurs at 212°C, leading to an abrupt drop in the mass (ca. 40%) and suggesting the beginning of the decomposition. Finally, a decomposition of more than 70% is observed at 400°C.

The Derivative Thermogravimetry (DTG) curves of raw materials (AZM and excipients) and spray-dried AZM-PCL-MPs are shown in (Figure 4B). The thermal stability of PCL and Pluronic F127 were observed in the thermal degradation pattern of the spray-dried formulation AZM-PCL-MP indicating that both polymers retained their original thermal behavior in the microparticles. PCL and Pluronic F127 showed a clear degradation peak temperature at 410°C and 388°C, respectively, confirmed by Ramírez-Agudelo et al. [43]. AZM thermogram showed a thermal degradation at 260°C, in agreement with values reported by Maswadeh et al. [37]. According to the DTG results, the thermal degradation of AZM-PCL-MP could be divided into three stages. The first stage is associated to the intermolecular water loss around 136°C. The second stage at 220°C is attributed at the degradation of LH206, which is in higher proportion in the AZM-PCL-MP formulation. The third stage is assigned to the decomposition of the AZM-PCL-MP formulation at 400°C. Data obtained by DSC not only corroborate with the TGA, but also present first order phase transitions (melting temperature), indicating the high degree of purity of the microparticles produced.

X-ray powder diffraction (XRPD)

X-ray powder diffraction was used to evaluate the solid-state properties of both raw materials (AZM and excipients) and spray-dried AZM-PCL-MPs (Figure 5). Data on the crystal lattice parameters of AZM have already been described in the literature [44]. AZM at room temperature is an orthorhombic

FIGURE 4
(A) Thermogravimetric analysis (TGA) and **(B)** DTG curves of azithromycin (AZM), lactose monohydrate (LH206), polycaprolactone (PCL), pluronicF127 and dried AZM-PCL-MP formulation.

FIGURE 5
X-ray diffraction of azithromycin (AZM), lactose LH206, polycaprolactone (PCL), PluronicF127, dipalmitoylphosphatidylcholine (DPPC) and spray-dried formulations (PCL-MPs and AZM-PCL-MPs).

structure, and belongs to the space group P21, a = 14.735 Å, b = 16.844 Å, c = 17.810 Å, α = 90°, β = 90°, γ = 90°, describing the crystallinity of AZM.

In this work, the AZM diffractogram showed an intense peak at 10.06° (2θ) and other sharp peaks at 16.62°, 17.80°, 18.88° and 19.96° (2θ), highlighting the crystallinity of the drug as studied by [5], where similar peaks were obtained for AZM encapsulated by poly-lactic acid (PLA). PCL and Pluronic F127 exhibited the characteristics of a semicrystalline polymer and copolymer, respectively, with two broad peaks

at 21.36°; 23.78° and 19.28°; 23.46° (2θ), respectively. These peaks were also found for other research using PCL and chitosan nanofibers with encapsulated AZM [40]. Lactose LH206 appeared as a crystalline material, with an intense peak at 20.12° 2θ and the presence of some peaks with lower intensity at 12.68°, 19.28° and 21.38° (2θ). On the other hand, in the DPPC, a diffraction pattern without peaks and in a disorganized form can be observed, demonstrating the amorphous structure of this raw material.

For PCL-MPs and AZM-PCL-MPs, they showed a peak with greater intensity at 20° and 20.1° (2θ), and other peaks with lower intensity were observed at 12.5° and 19.2° (2θ), which are attributed to lactose LH206. Furthermore, both powder formulations (PCL-MPs and AZM-PCL-MPs) exhibited diffraction patterns similar to those obtained for PCL (21.48° 2θ) and Pluronic F127 (23.1° 2θ) raw materials. However, no peaks were observed for AZM (10.06° 2θ), indicating that AZM is preferably dispersed in the polymeric nanoparticle matrix [33].

ATR-FTIR measurements

According to (Figure 6A, the spectrum of Pluronic F127, showed the main stretching of aliphatic bands (C-H) around 2,882 cm^{-1} and symmetric C-O-C stretching at 1,104 cm^{-1}, already reported in literature [45]. Lactose LH206 showed the stretching vibration of the hydroxyl group (OH) at 3,667 cm^{-1} and the characteristic bands at 2,989 cm^{-1} and 2,898 cm^{-1} attributed to the asymmetric and symmetric stretching vibrations of the CH$_2$, respectively [46]. The FTIR spectrum of DPPC presented the principal band between 3,600 cm^{-1} and 3,700 cm^{-1}, which indicates the vibration of the OH group. Asymmetric and symmetric vibration at 2,931 cm^{-1} and 2,852 cm^{-1} were observed and attributed to the CH$_2$ group. The band at 1736 cm^{-1} clearly
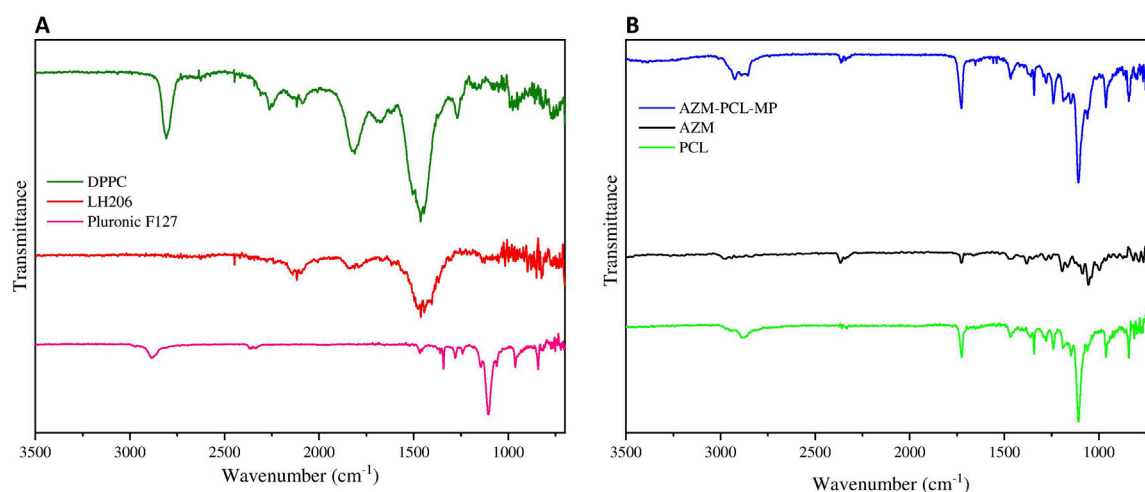
FIGURE 6
(A) FTIR spectrum of Pluronic F127, lactose monohydrate (LH206), phospholipid (DPPC), **(B)** FTIR spectrum of PCL, AZM and spray-dried AZM-PCL-MP formulation.

represents the carbonyl stretching. The stretching vibrations of the phosphate group were observed in the range of 1,230 cm^{-1} and 1,190 cm^{-1}. In addition, the band at 1,050 cm^{-1} refers to the vibrations of the CO-PO$_2$ group vibrations [47].

In Figure 6B, the spectrum of AZM showed a band in the range of 3,559 cm^{-1} and 3,488 cm^{-1}, attributed to the vibration of N-H group [37]. Furthermore, The CH$_2$ groups were also confirmed by the asymmetric and symmetric vibrations bands at 2,974 cm^{-1} and 2,898 cm^{-1}, respectively [48]. The band at 1,721 cm^{-1} confirmed the vibration of the carbonyl group. Other bands between 1,123 cm^{-1} and 1,250 cm^{-1} suggested the absorption associated with axial stretching of the C-O functional group [49].

The FTIR spectrum of PCL (Figure 6B) has a characteristic band at 2,950 cm^{-1} indicating the asymmetric CH$_2$ stretching and symmetric CH$_2$ stretching at 2,880 cm^{-1}. The band at 1,723 cm^{-1} represents the carbonyl stretching and the 1,108 cm^{-1} was attributed to the symmetric C-O-C stretching [50].

Comparing the FTIR spectra of the raw materials and the AZM-PCL-MP formulation (Figures 6A, B), we can see that the characteristic band of AZM was present in the formulation spectra. For AZM-PCL-MPs (Figure 6B) spectra, not only the carbonyl group at 1,725 cm^{-1} but also the asymmetric and symmetric stretching vibrations of CH$_2$ at 2,931 cm^{-1} and 2,852 cm^{-1} were observed. The band at 1,100 cm^{-1}corresponds to vibrations of C-O-C and were expected according to the raw materials. In addition, the displacement of the bands corresponding to the AZM for AZM-PCL-MPs indicated the formation of microparticles in which the drug was molecularly dispersed [5].

Particle size distribution
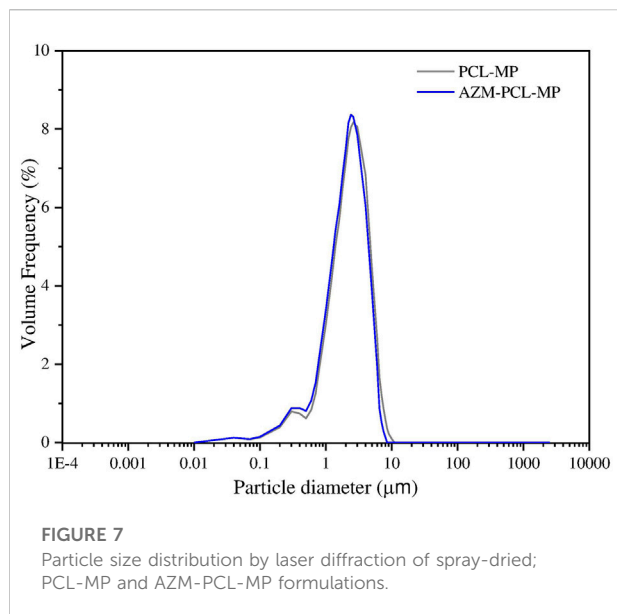
The particle size distribution of PCL-MP and AZM-PCL-MP formulations are showed in Figure 7. For the deep lung deposition of

inhalable dry powders, diameters in the range of 1–5 μm are required [51]. In this study, 90% (d$_{90}$) of the AZM-PCL-MPs presented a size of 4.06 μm, or smaller which may result in successful deposition in the deeper airways. This particle size distribution can be related to the lower concentration of PCL used during the emulsification process, which consequently results in smaller microparticles when dried by spray-drying process. When the PCL concentration is reduced in the emulsification step, the viscosity of the organic phase decreases, leading to a smaller droplet size due to more efficient dispersion and breakup during emulsification step. This effect is consistent with observations made by Balmayor et al., who reported that lower PCL concentrations lead to a decrease in the size of microparticles formed during the emulsification process. In the spray-drying process, rapid solvent evaporation solidifies the droplets, fixing the microparticle size [52]. Since PCL has a relatively low glass transition temperature and is flexible, it supports the formation of small, spherical particles when processed under optimal conditions [53].

The particle size distribution of powder formulation is summarized in Table 2. As can be seen, volume median diameter (d$_{0.5}$) and volume mean diameter (d$_{4.3}$) varied from 1.95 μm to 1.96 μm and 2.47 μm to 2.83 μm, respectively. Span values of 1.70–1.83 indicate homogenous size distributions, which is important for accurate dosing [54].

Particle morphology

The morphology of AZM, lactose LH206 and microparticles was investigated by SEM (Figure 8A) exhibited a slightly rough surface, in an aggregated disposition, with D > 10 μm. Spherical microparticles smaller than 5 μm and presenting a rough and highly porous surface were observed in lactose after spray-drying (Figure 8B).

FIGURE 7
Particle size distribution by laser diffraction of spray-dried; PCL-MP and AZM-PCL-MP formulations.

using an NGI. AZM-PCL-MPs was deposited successfully in all stages (1–7), while AZM was deposited just at the first stages (1–3). As seen in Table 3, mass median aerodynamic diameter (MMAD) values are remarkably different for AZM and AZM-PCL-MP, 12.34 μm and 5.13 μm, respectively, and MMAD values between 1 and 5 μm are preferable for reaching depth in the lungs. These results are similar to other inhalable dry powders prepared by conventional spray-drying technique [6]. According to the aerosol dispersion performance parameters, AZM-PCL-MP, displayed a fine particle fraction (FPF) around 55% indicating good aerosolization characteristics and suitability for oral inhalation and lung delivery. In contrast, the AZM presented lower values of ED, FPF and RF when compared with AZM-PCL-MP, which we attributed to the aggregates and higher aerodynamic diameter of AZM (ca. 12 μm), leading to reduced FPF and RF values.

Cytotoxicity assay

Since the microparticles can be inhaled orally, they may directly interact with lung cells. As primary assessment, we used MTT assay to verify whether our formulations and its components trigger cellular toxicity. Consequently, human cell lines BEAS-2B (lung epithelial), HUVEC (endothelial) and HFF1 (fibroblasts) were exposed to a wide range of AZM concentrations (25–1,600 μg/mL) either free or incorporated into nanoparticles during 24 h. The results of the MTT assay are summarized in (Figure 9). As can be seen, HUVEC (Figure 9B) and HFF-1 (Figure 9C) were more susceptible to the free AZM with 30%–40% of cell viability compared to BEAS-2B cells (Figure 9A) with 80–100% of cell viability at the highest concentrations (120–1,600 μg/mL). Rampacci et al. [56] also demonstrated a dose-dependent viability of BEAS-2B cells to AZM.

The placebo PCL-NPs showed very compatible with HUVEC (Figure 9B) and HFF-1 (Figure 9C) cells, with viability around 100% at concentrations up to 800 μg/mL. BEAS-2B cells (Figure 9A), on the other hand, presented some sensitivity to the PCL-NPs, nonetheless up to 70% of cell viability was preserved at concentrations up to 150 μg/mL. Thus, the good biocompatibility of PCL makes this biopolymer an appropriate carrier for drug delivery [47].

Notably, the obtained AZM-PCL-MPs and PCL-MPs present a nearly spherical shape < 5 μm (Figures 8C, D). The microparticles presented shapeless surface, as expected for a complex mixture including DPPC phospholipids, polymers (PCL and Pluronic F127), AZM and lactose LH206. Other authors showed uneven particles and aggregation when adding different types of drying aids such as mannitol or leucine into polymeric formulations [32]. Rough surfaces were predominantly observed in our spray-dried formulations, which is preferred for pulmonary delivery since it tends to increase the aerosolization efficiency [49].

Overall, the particles obtained in this work showed a proper powder dispersion, which can result in an optimal inhalation profile and, therefore, higher drug delivery into the deeper airways [55].

Aerodynamic performance by NGI

Microparticles for oral inhalation must have adequate aerodynamic behavior. Therefore, the aerodynamic properties of AZM and AZM-PCL-MPs were characterized

TABLE 2 Particle size of spray-dried formulations.

Sample formulation	Particle size distribution[a]				
	$d_{0.1}$ (μm)	$d_{0.5}$ (μm)	$d_{0.9}$ (μm)	$d_{4.3}$ (μm)[b]	Span
PCL-MP	0.46 ± 0.03	1.95 ± 0.01	4.03 ± 0.33	2.47	1.83
AZM-PCL-MP	0.72 ± 0.03	1.96 ± 0.01	4.06 ± 0.49	2.86	1.70

Data are means ± SD (n = 3 independent measurements).
Mean ± standard deviation (SD).
[a]Equivalent volume diameters at 10% ($d_{0.1}$), 50% ($d_{0.5}$), and 90% ($d_{0.9}$) cumulative volume.
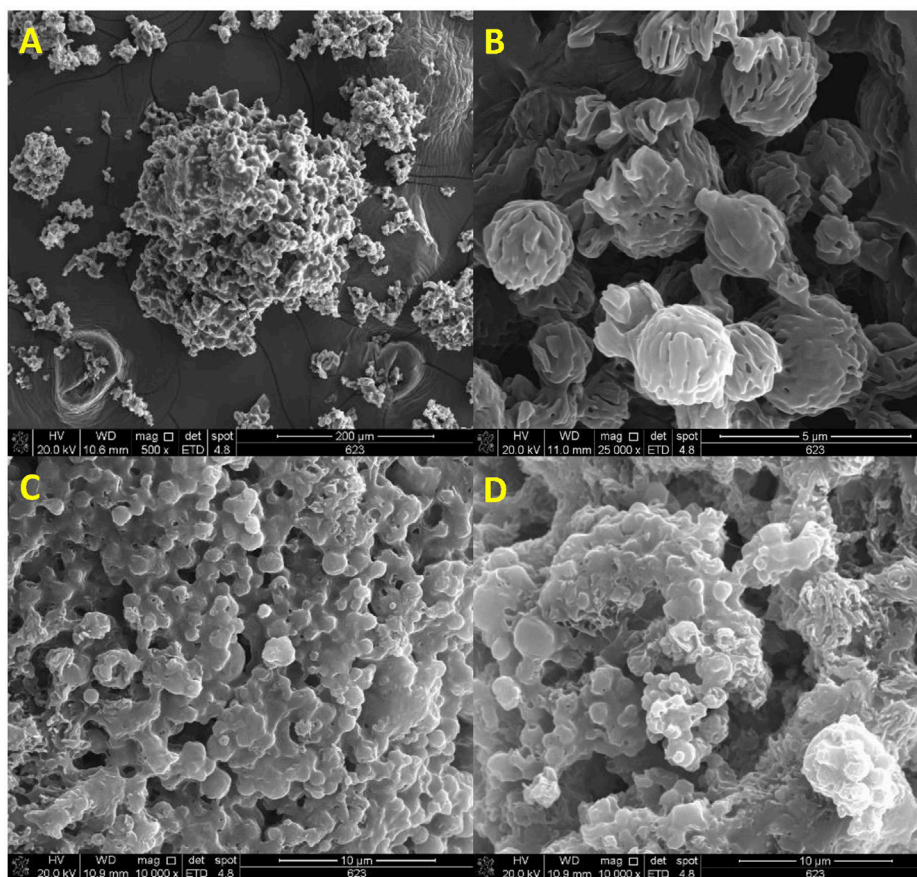[b]Volume mean diameter.

FIGURE 8
SEM micrographs of **(A)** azithromycin (AZM), **(B)** spray-dried lactose LH206, **(C)** spray-dried AZM–PCL-MP formulation, **(D)** spray-dried PCL-MP formulation.

TABLE 3 Aerodynamic properties of AZM and AZM-PCL-MPs determined by next-generation impactor (NGI) including emitted dose (ED, %), fine particle fraction (FPF, %), respirable fraction (RF, %) and Mass Median Aerodynamic Diameter (MMAD, μm).

Powder	Aerosol dispersion performance parameters			
	ED (%)	FPF (%)	RF (%)	MMAD (μm)
AZM	44	15	8	12.32
AZM-PCL-MP	87	55	42	5.13

For AZM-PCL-NPs toxicity higher than 40% was already observed for 25 μg/mL were BEAS-2B cells (Figure 9A), indicating the nanostructures might have promoted the intracellular drug delivery. The same effect was observed in HUVEC (Figure 9B) and HFF-1 (Figure 9C) for concentrations up to 100 μg/mL of AZM loaded in the PCL-NPs. Above this concentration, the AZM was found to be in general more toxic than the AZM-PCL-NPs. Therefore, there should be a balance between the drug and the nanostructures toxicity.

Antibacterial activity

Halos formation by *S. aureus* and *S. Pneumoniae* were observed at all concentrations tested for AZM-PCL-NP and AZM (Table 4). Halos below 13 mm indicate resistance and halos ≥13 mm indicate sensibility to AZM. As can be seen in (Table 4), halos ≥18 mm were formed in *S. aureus* and *S. Pneumoniae* in the presence of AZM-PCL-NP. No significant differences were observed between the halos formed with AZM and AZM-PCL-NP, therefore both strains could in principle be adequately treated with AZM-PCL-NP.

Nanoparticles can improve drug permeability across the cell membrane enhancing intracellular accumulation, antibacterial activity against the resistant strains, offering multiple bactericidal mechanisms, and inhibiting the biofilm formation by *S. aureus* [57]. Thus, the AZM-PCL-NP delivery system we developed presents strong potential to overcome the challenges associated to the treatment of *S. aureus* and *S. pneumoniae* infections.
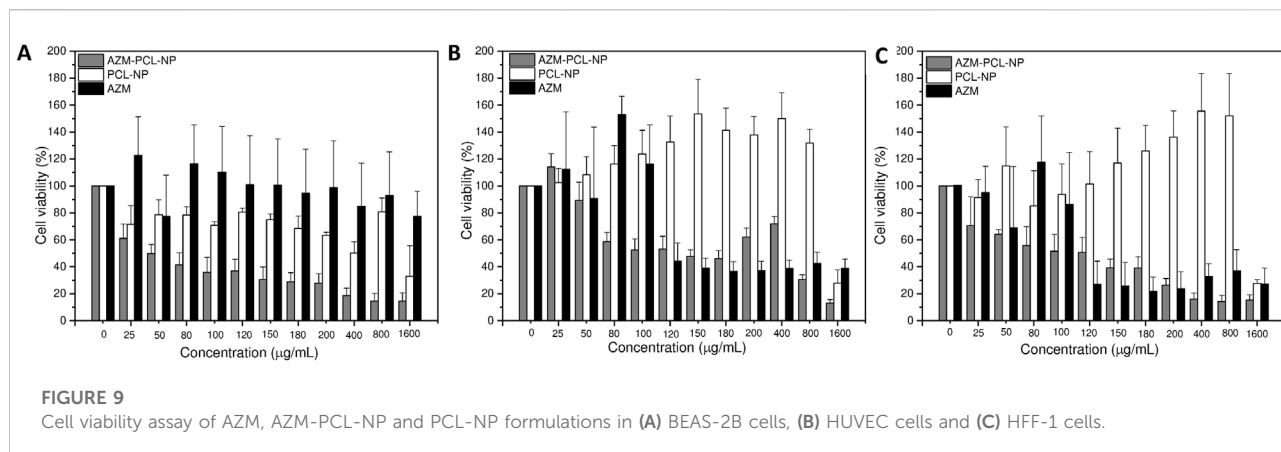
FIGURE 9
Cell viability assay of AZM, AZM-PCL-NP and PCL-NP formulations in **(A)** BEAS-2B cells, **(B)** HUVEC cells and **(C)** HFF-1 cells.

TABLE 4 Antimicrobial activity for AZM and AZM-PCL-NPs disk diffusion test against *S. aureus* and *S. pneumoniae*.

AZM concentration (µg/mL)	*S. aureus*		*S. pneumoniae*	
	AZM-PCL-NP D_{Halo} (mm)	AZM D_{Halo} (mm)	AZM-PCL-NP D_{Halo} (mm)	AZM DHalo (mm)
1,600	26.0 ± 1.0	25.0 ± 1.0	38.0 ± 2.0	36.0 ± 0.0
800	24.7 ± 0.6	24.0 ± 1.0	35.0 ± 1.0	34.7 ± 0.6
400	23.0 ± 1.0	21.0 ± 0.0	31.7 ± 0.6	31.0 ± 2.0
200	22.0 ± 1.0	20.3 ± 0.6	28.3 ± 0.6	29.3 ± 0.6
100	19.0 ± 1.0	19.3 ± 0.6	25.3 ± 0.6	25.0 ± 1.0
50	18.0 ± 1.0	16.7 ± 0.6	24.0 ± 2.0	22.0 ± 2.0

D_{halo} = diameter of inhibition halo. Mean ± standard deviation (SD).

TABLE 5 Bacterial viability test of AZM, PLC-NP and AZM-PCL-NP formulations in *S. aureus* and *S. pneumoniae*.

AZM (µg/mL)	*S. aureus*			*S. pneumoniae*		
	AZM-PCL-NP	AZM	PCL-NP	AZM-PCL-NP	AZM	PCL-NP
0	V	V	V	V	V	V
50	NV	NV	NV	NV	NV	NV
100	NV	NV	V	NV	NV	V
200	NV	NV	V	NV	NV	V
400	NV	NV	V	NV	NV	V
800	NV	NV	V	NV	NV	V
1,600	NV	NV	V	NV	NV	V

V: Viable cell (reduced)/NV: Non-viable cell (oxidized state).

Bacterial viability

After demonstrating growth inhibition of *S. aureus* and *S. pneumoniae*, the antibacterial effect of AZM, either free or incorporated into nanoparticles formulations was evaluated by resazurin bacterial susceptibility test. The resazurin reduction assay depends on the ability of metabolically active cells to reduce the resazurin redox dye to resorufin and is used to determine viability in bacterial cells [58]. After 24 h of each treatment and 1 h of incubation with resazurin, non-viable cells were observed,

with an oxidized state through the detection of the blue color reaching the same results both in *S. aureus* and in *S. pneumoniae* bacteria (Table 5).

Finally, the minimum concentration required to inhibit growth (MIC) of both strains *S. aureus* and *S. pneumoniae* was found to be 3 μg/mL of AZM-PCL-NPs. No cell growth was observed after treatment with free AZM. On the other hand, bacteria with placebo (PCL-NPs) resulted in colony formation.

Conclusion

In this work, spherical and homogenous AZM-loaded PCL nanoparticles functionalized with DPPC were produced by the emulsion/solvent diffusion-evaporation method. Our formulation preserves the antimicrobial effect of AZM against *S. aureus* and *S. pneumoniae*, two important pathogens of the respiratory tract. Besides, the formulation did not trigger acute cytotoxicity to human endothelial, pulmonary, and fibroblast cell lines. The colloidal dispersion (AZM-PCL-NP) was stable at 4°C up to 6 months in terms of small hydrodynamic diameter and narrow monomodal size distribution and was further used to prepare a dry powder of adequate size for pulmonary delivery through spray-drying. The aerosolizable microparticles formulation (AZM-PCL-MP) was obtained as a white homogenous powder of adequate size for pulmonary delivery with optimal aerosolization properties. Also, the dry powder formulation was characterized by thermal analysis and no degradation or reaction of the components was observed at room temperature. Thus, the AZM-PCL-MPs developed present optimized physicochemical properties that can ensure the successful aerosolization and deposition of dry powder in the lungs and, therefore, can be tested as a novel platform to deliver antibiotics for lung infections. In summary, we produced a potential alternative to treat respiratory tract infections by inhalation therapy.

Data availability statement

The original contributions presented in the study are included in the article/supplementary material, further inquiries can be directed to the corresponding authors.

Ethics statement

Ethical approval was not required for the studies on humans in accordance with the local legislation and institutional requirements because only commercially available established cell lines were used. Ethical approval was not required for the studies on animals in accordance with the local legislation and institutional requirements because only commercially available established cell lines were used.

Author contributions

AM, KR-R, MS, and MC designed the experimental study. AM drafted the manuscript. HR, PL, NC, MZ, VF, and CR-Y, reviewed the manuscript. All authors contributed to the article and approved the submitted version.

Funding

Acknowledgments

Conflict of interest

The authors declare that the research was conducted in the absence of any commercial or financial relationships that could be construed as a potential conflict of interest.

Generative AI statement

The author(s) declare that no Generative AI was used in the creation of this manuscript.

References

1. Liu M, Jia X, Liu H, He R, Zhang X, Shao Y, et al. Role of TRPV1 in respiratory disease and association with traditional Chinese medicine: a literature review. *Biomed & Pharmacother* (2022) 155:113676. doi:10.1016/j.biopha.2022.113676

2. Smith MD, Fee C, Mace SE, Maughan B, Perkins JC, Jr, Kaji A, et al. Clinical policy: critical issues in the management of adult patients presenting to the emergency department with community-acquired pneumonia. *Ann Emerg Med* (2021) 77:e1–57. doi:10.1016/j.annemergmed.2020.10.024

3. Yan Y, Tomooka K, Naito T, Tanigawa T. Decreased number of inpatients with community-acquired pneumonia during the COVID-19 pandemic: a large multicenter study in Japan. *J Infect Chemother* (2022) 28:709–13. doi:10.1016/j.jiac.2022.01.013

4. Hinks TSC, Cureton L, Knight R, Wang A, Cane JL, Barber VS, et al. Azithromycin versus standard care in patients with mild-to-moderate COVID-19 (ATOMIC2): an open-label, randomised trial. *Lancet Respir Med* (2021) 9:1130–40. doi:10.1016/S2213-2600(21)00263-0

5. Li X, Chang S, Du G, Li Y, Gong J, Wei Z, et al. Encapsulation of azithromycin into polymeric microspheres by reduced pressure-solvent evaporation method. *Int J Pharmaceutics* (2012) 433:79–88. doi:10.1016/j.ijpharm.2012.04.081

6. Feng J, Cao D, Zheng D, Qian ZM, Huang C, Shen H, et al. Cold spells linked with respiratory disease hospitalization, length of hospital stay, and hospital expenses: exploring cumulative and harvesting effects. *Sci Total Environ* (2023) 863:160726. doi:10.1016/j.scitotenv.2022.160726

7. Ballow CH, Amsden GW. Azithromycin: the first azalide antibiotic. *Ann Pharmacother* (1992) 26:1253–61. doi:10.1177/106002809202601014

8. Martinez MA, Vuppalanchi R, Fontana RJ, Stolz A, Kleiner DE, Gu J, et al. Clinical and histologic features of azithromycin-induced liver injury. *Clin Gastroenterol Hepatol* (2015) 13:369–76.e3. doi:10.1016/j.cgh.2014.07.054

9. Yang Z, Prinsen JK, Bersell KR, Shen W, Yermalitskaya L, Luis PB, et al. Azithromycin causes a novel proarrhythmic syndrome. *Circ Arrhythm Electrophysiol* (2017) 10:e003560–12. doi:10.1161/CIRCEP.115.003560

10. Al-Jazairi AS, Alotaibi HS. Possible azithromycin-induced life-threatening arrhythmia requiring extracorporeal membrane oxygenation support: a case report. *Am J Case Rep* (2020) 21:e926951–5. doi:10.12659/AJCR.926951

11. Parvathaneni V, Kulkarni NS, Shukla SK, Farrales PT, Kunda NK, Gupta V, et al. Systematic development and optimization of inhalable pirfenidone liposomes for non-small cell lung cancer treatment. *Pharmaceutics* (2020) 12:206. doi:10.3390/pharmaceutics12030206

12. Lechanteur A, Evrard B. Influence of composition and spray-drying process parameters on carrier-free DPI properties and behaviors in the lung: a review. *Pharmaceutics* (2020) 12:55. doi:10.3390/pharmaceutics12010055

13. Chaurasiya B, Zhao YY. Dry powder for pulmonary delivery: a comprehensive review. *Pharmaceutics* (2020) 13:31–28. doi:10.3390/pharmaceutics13010031

14. Ambrus R, Benke E, Farkas Á, Balásházy I, Szabó-Révész P. Novel dry powder inhaler formulation containing antibiotic using combined technology to improve aerodynamic properties. *Eur J Pharm Sci* (2018) 123:20–7. doi:10.1016/j.ejps.2018.07.030

15. Sibum I, Hagedoorn P, Frijlink HW, Grasmeijer F. Characterization and formulation of isoniazid for high-dose dry powder inhalation. *Pharmaceutics* (2019) 11:233. doi:10.3390/pharmaceutics11050233

16. Sultana N, Arayne MS, Hussain F, Fatima A. Degradation studies of azithromycin and its spectrophotometric determination in pharmaceutical dosage forms. *Pak J Pharm Sci* (2006) 19:98–103.

17. Hamzehloo M, Karimi J, Eghbali N, Mirzakhani M, Aghapoor K, Darabi HR, et al. A new blend of polymeric encapsulation of azithromycin by spray-drying with a pH responsive in drug release. *Drying Technol* (2017) 35:1688–95. doi:10.1080/07373937.2016.1269807

18. Ma Z, Milton-mcgurk L, Tang P, Chan H, Farina D, Cheng S, et al. An experimental study of the effect of individual upper airway anatomical features on the deposition of dry powder inhaler formulations. *J Aerosol Sci* (2024) 177:106320. doi:10.1016/j.jaerosci.2023.106320

19. Mosmann T. Rapid colorimetric assay for cellular growth and survival: application to proliferation and cytotoxicity assays. *J Immunological Methods* (1983) 65:55–63. doi:10.1016/0022-1759(83)90303-4

20. Suárez N, Texeira E. Optimal conditions for Streptococcus pneumoniae culture: in solid and liquid media. *Methods Mol Biol* (2019) 1968:3–10. doi:10.1007/978-1-4939-9199-0_1

21. e Silva SS, Carvalho JWP, Aires CP, Nitschke M. Disruption of *Staphylococcus aureus* biofilms using rhamnolipid biosurfactants. *J Dairy Sci* (2017) 100:7864–73. doi:10.3168/jds.2017-13012

22. Salomoni R, Léo P, Montemor AF, Rinaldi BG, Rodrigues MFA. Antibacterial effect of silver nanoparticles in *Pseudomonas aeruginosa*. *Nanotechnology, Sci Appl* (2017) 10:115–21. doi:10.2147/NSA.S133415

23. Ribeiro MO, Gomes Md S, Senna SG, Rossetti MLR, Fonseca Ld S. Avaliação de testes rápidos em microplacas usando indicadores de viabilidade celular para determinação da susceptibilidade de cepas de *Mycobacterium tuberculosis* à isoniazida e rifampicina. *J Bras Pneumol* (2004) 30:365–70. doi:10.1590/s1806-37132004000400011

24. Castilho AL, Caleffi-Ferracioli KR, Canezin PH, Dias Siqueira VL, de Lima Scodro RB, Cardoso RF, et al. Detection of drug susceptibility in rapidly growing mycobacteria by resazurin broth microdilution assay. *J Microbiol Methods* (2015) 111:119–21. doi:10.1016/j.mimet.2015.02.007

25. Cruz CD, Shah S, Tammela P. Defining conditions for biofilm inhibition and eradication assays for Gram-positive clinical reference strains. *BMC Microbiol* (2018) 18:173–9. doi:10.1186/s12866-018-1321-6

26. Buhecha MD, Lansley AB, Somavarapu S, Pannala AS. Development and characterization of PLA nanoparticles for pulmonary drug delivery: co-encapsulation of theophylline and budesonide, a hydrophilic and lipophilic drug. *J Drug Deliv Sci Technol* (2019) 53:101128. doi:10.1016/j.jddst.2019.101128

27. Quintanar-Guerrero D, Allémann E, Fessi H, Doelker E. Preparation techniques and mechanisms of formation of biodegradable nanoparticles from preformed polymers. *Drug Develop Ind Pharm* (1998) 24:1113–28. doi:10.3109/03639049809108571

28. Galindo-Rodriguez S, Allémann E, Fessi H, Doelker E. Physicochemical parameters associated with nanoparticle formation in the salting-out, emulsification-diffusion, and nanoprecipitation methods. *Pharm Res* (2004) 21:1428–39. doi:10.1023/B:PHAM.0000036917.75634.be

29. Ferreira IJ, de Menezes LR, Tavares MIB. Obtaining PCL/tea tree oil particles with antimicrobial capacity and high cytocompatibility. *Polym Bull* (2024). doi:10.1007/s00289-024-05455-y

30. Yu J, Qiu H, Yin S, Wang H, Li Y. Polymeric drug delivery system based on pluronics for cancer treatment. *Molecules* (2021) 26:3610–23. doi:10.3390/molecules26123610

31. Nwazojie CC, Obayemi JD, Salifu AA, Borbor-Sawyer SM, Uzonwanne VO, Akpan UM, et al. Targeted drug-loaded PLGA-PCL microspheres for specific and localized treatment of triple negative breast cancer. *J Mater Sci Mater Med* (2023) 34:41. doi:10.1007/s10856-023-06738-y

32. Mangal S, Nie H, Xu R, Guo R, Cavallaro A, Zhou Q, et al. Physico-chemical properties, aerosolization and dissolution of co-spray dried azithromycin particles with L-leucine for inhalation. *Pharm Res* (2018) 35:28. doi:10.1007/s11095-017-2334-9

33. Haggag YA, Faheem AM. Evaluation of nano spray drying as a method for drying and formulation of therapeutic peptides and proteins. *Front Pharmacol* (2015) 6:140–5. doi:10.3389/fphar.2015.00140

34. Cotabarren IM, Bertín D, Razuc M, Ramírez-Rigo MV, Piña J. Modelling of the spray drying process for particle design. *Chem Eng Res Des* (2018) 132:1091–104. doi:10.1016/j.cherd.2018.01.012

35. Mohamady Hussein MA, Guler E, Rayaman E, Cam ME, Sahin A, Sezgin Mansuroglu D, et al. Dual-drug delivery of Ag-chitosan nanoparticles and phenytoin via core-shell PVA/PCL electrospun nanofibers. *Carbohydr Polym* (2021) 270:118373. doi:10.1016/j.carbpol.2021.118373

36. Karolewicz B, Górniak A, Owczarek A, Zurawska-Płaksej E, Piwowar A, Pluta J, et al. Thermal, spectroscopic, and dissolution studies of ketoconazole-pluronic F127 system. *J Therm Anal Calorim* (2014) 115:2487–93. doi:10.1007/s10973-014-3661-2

37. Eedara BB, Rangnekar B, Doyle C, Cavallaro A, Das SC. The influence of surface active L-leucine and 1,2-dipalmitoyl-sn-glycero-3-phosphatidylcholine (DPPC) in the improvement of aerosolization of pyrazinamide and moxifloxacin co-spray dried powders. *Int J Pharmaceutics* (2018) 542:72–81. doi:10.1016/j.ijpharm.2018.03.005

38. Listiohadi Y, Hourigan JA, Sleigh RW, Steele RJ. Thermal analysis of amorphous lactose and α-lactose monohydrate. *Dairy Sci Technol* (2009) 89:43–67. doi:10.1051/dst:2008027

39. Maswadeh H. Incompatibility of paracetamol with pediatric suspensions containing amoxicillin, azithromycin and cefuroxime axetil. *Pharmacol Pharm* (2017) 08:355–68. doi:10.4236/pp.2017.811026

40. Sánchez-Aguinagalde O, Meaurio E, Lejardi A, Sarasua JR. Amorphous solid dispersions in poly(ε-caprolactone)/xanthohumol bioactive blends: physicochemical and mechanical characterization. *J Mater Chem B* (2021) 9:4219–29. doi:10.1039/d0tb02964e

41. Agalloco JP, Augsburger LL, Bergstrom DH, Borman P, Schoneker DR, Srinivasan A, et al. *Pharmaceutical technology*. 7th ed. NJ, USA: Pharmatech (2017).

42. Garnier S, Petit S, Mallet F, Petit MN, Lemarchand D, Coste S, et al. Influence of ageing, grinding and preheating on the thermal behaviour of α-lactose monohydrate. *Int J Pharmaceutics* (2008) 361:131–40. doi:10.1016/j.ijpharm.2008.05.023

43. Ramírez-Agudelo R, Scheuermann K, Gala-García A, Monteiro APF, Pinzón-García AD, Sinisterra RD, et al. Hybrid nanofibers based on poly-caprolactone/gelatin/hydroxyapatite nanoparticles-loaded Doxycycline: effective anti-tumoral and antibacterial activity. *Mater Sci Eng C* (2018) 83:25–34. doi:10.1016/j.msec.2017.08.012

44. Alimohammadi M, Fakhraei O, Moradi A, Kabiri M, Moradi A, Tamayol A, et al. Controlled release of azithromycin from polycaprolactone/chitosan nanofibrous membranes. *J Drug Deliv Sci Technol* (2022) 71:103246. doi:10.1016/j.jddst.2022.103246

45. Al Kayal T, Panetta D, Canciani B, Losi P, Tripodi M, Burchielli S, et al. Evaluation of the effect of a gamma irradiated DBM-pluronic F127 composite on bone regeneration in wistar rat. *PLoS One* (2015) 10:e0125110. doi:10.1371/journal.pone.0125110

46. Rashid MA, Elgied AA, Alhamhoom Y, Chan E, Rintoul L, Islam N, et al. Excipient interactions in glucagon dry powder inhaler formulation for pulmonary delivery. *Pharmaceutics* (2019) 11:207. doi:10.3390/pharmaceutics11050207

47. Mohan V, Naske CD, Britten CN, Karimi L, Walters KB. Hydroxide-catalyzed cleavage of selective ester bonds in phosphatidylcholine: an FTIR study. *Vibrational Spectrosc* (2020) 109:103055. doi:10.1016/j.vibspec.2020.103055

48. Islam MR, Moghal MMR, Bari FSNU, Mamun EA. Design and development of Bi-layered sustained release azithromycin tablets. *Dhaka Univ J Pharm Sci* (2017) 15:227–34. doi:10.3329/dujps.v15i2.30942

49. Adeli E. The use of spray freeze drying for dissolution and oral bioavailability improvement of Azithromycin. *Powder Technol* (2017) 319:323–31. doi:10.1016/j.powtec.2017.06.043

50. Soni G, Yadav KS, Gupta MK. QbD based approach for formulation development of spray dried microparticles of erlotinib hydrochloride for sustained release. *J Drug Deliv Sci Technol* (2020) 57:101684. doi:10.1016/j.jddst.2020.101684

51. Ungaro F, d'Emmanuele di Villa Bianca R, Giovino C, Miro A, Sorrentino R, La Rotonda MI, et al. Insulin-loaded PLGA/cyclodextrin large porous particles with improved aerosolization properties: *in vivo* deposition and hypoglycaemic activity after delivery to rat lungs. *J Controlled Release* (2009) 135:25–34. doi:10.1016/j.jconrel.2008.12.011

52. Malamatari M, Charisi A, Malamataris S, Kachrimanis K, Nikolakakis I. Spray drying for the preparation of nanoparticle-based drug formulations as dry powders for inhalation. *Processes* (2020) 8:788. doi:10.3390/pr8070788

53. Balmayor ER, Tuzlakoglu K, Azevedo HS, Reis RL. Preparation and characterization of starch-poly-ε-caprolactone microparticles incorporating bioactive agents for drug delivery and tissue engineering applications. *Acta Biomater* (2009) 5:1035–45. doi:10.1016/j.actbio.2008.11.006

54. Party P, Kókai D, Burián K, Nagy A, Hopp B, Ambrus R, et al. Development of extra-fine particles containing nanosized meloxicam for deep pulmonary delivery: *in vitro* aerodynamic and cell line measurements. *Eur J Pharm Sci* (2022) 176:106247. doi:10.1016/j.ejps.2022.106247

55. Chvatal A, Ambrus R, Party P, Katona G, Jójárt-Laczkovich O, Szabó-Révész P, et al. Formulation and comparison of spray dried non-porous and large porous particles containing meloxicam for pulmonary drug delivery. *Int J Pharmaceutics* (2019) 559:68–75. doi:10.1016/j.ijpharm.2019.01.034

56. Rampacci E, Marenzoni ML, Chiaradia E, Passamonti F, Ricci M, Pepe M, et al. *In vitro* performances of novel co-spray-dried azithromycin/rifampicin microparticles for Rhodococcus equi disease treatment. *Sci Rep* (2018) 8:12149–11. doi:10.1038/s41598-018-30715-z

57. Zhou K, Li C, Chen D, Pan Y, Tao Y, Qu W, et al. A review on nanosystems as an effective approach against infections of *Staphylococcus aureus*. *Int J Nanomedicine* (2018) 13:7333–47. doi:10.2147/IJN.S169935

58. Mehring A, Erdmann N, Walther J, Stiefelmaier J, Strieth D, Ulber R, et al. A simple and low-cost resazurin assay for vitality assessment across species. *J Biotechnol* (2021) 333:63–6. doi:10.1016/j.jbiotec.2021.04.010